Ionizing radiation as a powerful tool for modification of metallic nanostructures

K.K. Kadyrzhanov [*,1], A.L. Kozlovskiy [1,2], A.A. Mashentseva [2]

[1] *L.N. Gumilyov Eurasian National University, Astana, Kazakhstan*
[2] *Institute of Nuclear Physics, Ministry of Energy of the Republic of Kazakhstan, Almaty, Kazakhstan*

[*] *e-mail: kadyrzhanov1945@gmail.com*

This paper presents a case study of targeted modification of the structure and properties of zinc nanotubes ordered arrays by treatment with Xe^{+22} and Kr^{+17} swift heavy ions (SHI). Polyethylene terephthalate track-etched membranes (PET TeMs) with a pore density of (4×10^9) $ions/cm^2$ have been used as a template for electrochemical deposition of Zn. Scanning electron microscopy and energy dispersive analysis have been used for a comprehensive elucidation of the dimensionality, chemical composition of the synthesized samples. Dynamics of changes in the crystallite shape and orientation of NTs before and after irradiation has been studied by X-ray diffraction. Changes in conductive properties as a result of irradiation were discussed. After Xe^{+22} ions irradiation with a fluence of (1×10^{11}) m^{-2} or higher, the formation of loose areas in the structure of Zn NTs as a result of partial degradation of the crystal structure and, consequently, a decline in conductivity are observed. In case of Kr^{+17} ions, the increase in current conduction with the increase in fluence may be due to the increase in the current carriers.

Keywords: zinc nanotubes, ionizing radiation, conductivity, track-etched membranes, swift heavy ions.

Introduction

Ionizing radiation induced effects on the properties and structure of metallic nanostructures with great potential applications in optoelectronics, photoelectro-chemistry, catalysis, medicine, etc. has attracted considerable attention during the last few decades [1-3]. Nanostructures based device require long-term operation in fields of ionizing radiation, at high temperatures and in corrosive environments, therefore nanostructures should have high stability and sensitivity [4,5].

Structural damage to the nanostructure on exposure to high energy ion beams has been the general understanding but recent research has shown it to be also a tool for tailoring properties and changing the structure of nanomaterials in a controllable way [6]. Analysis of published data revealed that several comprehensive studies had been performed on the effect of accelerated light and heavy ions on the transport properties of carbon-silica molecular sieves synthesized in channels of track-etched polymer membranes. Results of investigation of Zn [7], Cu [8-10], copper oxide selenite [11] and $CdSeO_3$ [12] nanostructures irradiated with ions of very high energy (on the order of (2.5-4.0) MeV/nucleon) followed by studying the properties of metallic nanostructures without removing the polymer matrix were reported. The effect of low-energy beams of heavy accelerated ions on the

structure and transport properties of composite materials based on metal nanostructures and track-etched membranes has not been well experimentally studied [13].

In this paper, the changes in structural properties and conduction characteristics of zinc composites synthesized in a polyethylene terephthalate track-etched membranes (PET) caused by accelerated Xe^{+22} and Kr^{+17} ions with different fluencies. The choice of zinc as the material to be deposited into the template PET template was due to the unique properties of nanoscale forms of this metal. The area of application of nanostructured materials based on zinc and its oxide [14] ranges from solar energy converters [15] and storage batteries [16] to information carriers and biosensors [14,17].

Experimental

Chemicals. Zinc sulfate heptahydrate, ammonium chloride, sodium acetate, and ascorbic acid (from Sigma) were of the analytical or reagent grade and were used without further purification, as well as all other chemicals.

Polymer Template Preparation. Track-etched membranes were made of Hostaphan ® polyethylene terephthalate manufacture by Mitsubishi Polyester Film (Germany). The films were irradiated using a DC-60 heavy ion accelerator (Kazakhstan) with accelerated 1.75-MeV krypton ions at a fluence of (4×10^7) ion/cm^2. The membranes were etched according to the standard procedure of bilateral etching in a 2.2 M NaOH solution at (85 ± 1)°C; the pore size was (380 ± 10) nm according to gas porosimetry and scanning electron microscopy data.

Electrochemical Deposition of Zinc in PET TeMS. Electrochemical deposition in tracks of the polymer template matrix was carried out in the potentiostatic mode at a voltage of 1.75 V according to [13]. The electrolyte solution had the following composition: $ZnSO_4 \cdot 7H_2O$ (360 g/L), NH_4Cl (30 g/L), $NaC_2H_3O_2 \cdot 3H_2O$ (15 g/L), and $C_6H_8O_6$ (120 g/L). The growth of nanostructures was monitored by chronoamperometry with an Agilent 34410A multimeter. Since PET template matrices are dielectric, a gold layer with a thickness of no more than 10 nm to be is used as a working electrode (cathode) during electrochemical machining was deposited to create a conductive layer by magnetron sputtering in a vacuum.

Study of Structure and Properties of Zinc Nanotubes. Structural characteristics and elemental composition of the obtained NTs before and after irradiation were studied using a Hitachi TM3030 scanning electron microscope with a Bruker XFlash MIN SVE microanalysis system at an accelerating voltage of 15 kV. X-ray diffraction studies were performed using a D8 ADVANCE diffractometer (CuKα-radiation, graphite monochromator) with an X-ray tube operating at 40 kV, 40 mA. Diffraction patterns were recorded in the range of 2θ angles from 30° to 90° with a step size of 0.02°.

Irradiation of zinc nanotubes in PET matrix. Samples of Zn nanotubes were irradiated in polymer matrices on the DC-60 heavy-ion accelerator at the Astana branch of the Institute of Nuclear Physics with Xe^{+22} and Kr^{+17} ions at a fluence of (1×10^9) to (5×10^{11}) cm^{-2}.

To determine range of accelerated ions in metallic nanostructures, we performed the theoretical calculation of energy loss to electrons and nuclei of the nanostructures using the SRIM 2013 Pro program. According to the SRIM-2013

software calculations (For irradiation of PET film with krypton ions with an energy of 1.75 MeV/nucleon and total energy 147 MeV: only PET film with density 1.3093 g/cm^3 and thickness of 12.0 μm was considered as a target. And for SRIM calculation of zinc NTs in PET template the next target was used: the density of the zinc was 8.92 g/cm^3, the density for PET was 1.3093 g/cm^3, and the target thickness was 12 μm; the projected range of ion beam in samples with energies 1.75 MeV/nucleon was calculated and was found to be 12.42 μm for Xe^{+22} and 11.87 μm for Kr^{+17}.

Measurement of current-voltage characteristics of Zn nanotubes. Current-voltage curves (CVCs) were measured using an HP 66312A power supply and an Agilent 34401A multimeter. The CVC measuring setup was assembled as follows: a sample with deposited nanotubes was sandwiched between two metal plates so that the plates cover only the part of the film containing nanotubes. Then the plates were connected to the power supply with in-series connection of the multimeter. Since PET has dielectric properties, the PET matrix does not contribute to current-voltage characteristic over the entire voltage range examined.

Results and discussion

The synthesized nanowires of zinc were tested for their surface morphology by SEM. Figure 1 presents SEM images of the synthesized Zn NTs; all the resulting nanostructures are cylindrical and repeat the track geometry of template pores. Prepared nanostructures are hollow nanotubes, the height of which coincides with the thickness of the template matrix of 12 μm, and the diameter of nanotubes correspond to the pore diameter of (380 ± 10) nm, the inner diameters of Zn nantotubes were calculated to be (180 ± 5) nm and the wall thickness, (100 ± 2) nm.

The elemental composition of the Zn NTs, determined by energy dispersive X-ray (EDX) spectroscopy, indicates that monocomponent zinc NTs were formed. Figure 3 shows the two prominent peaks Zn at 1.01 keV and 8.63 keV.
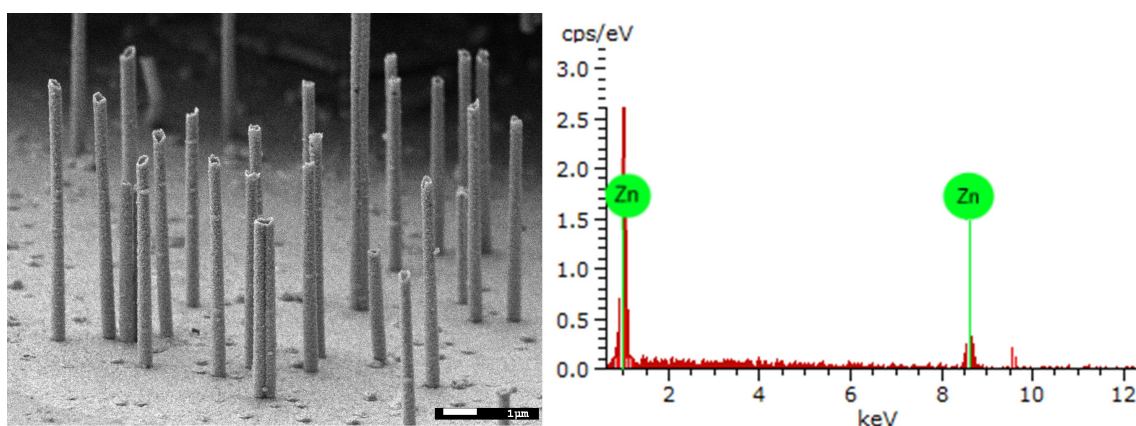

Figure 1. SEM images (a) and EDX spectra (b) of template-free Cu NTs electrochemically deposited on PET TeMs.

Ionizing radiation-induced change in the crystal structure of Zn NT samples was recorded using X-ray powder diffraction (XPD). It should be noted that the X-ray diffraction patterns of all the samples exhibited low-intensity peaks characteristic of diffraction of nanoscale objects (Figure 2). The X-ray analysis confirmed that the initial sample consists of Zn with the primitive hexagonal phase having

the following unit cell parameters: a = 2.6638 Å, c = 4.9337 Å. Analysis of the observed (002), (100), (101), (112), (200), (201), and (203) peaks showed that these Zn nanotubes are polycrystalline structures with the dominant texture plane [101]. There was no inception of new peak and was no shifting of peaks in the XRD spectra which revealed that nanotubes were not oxidized.
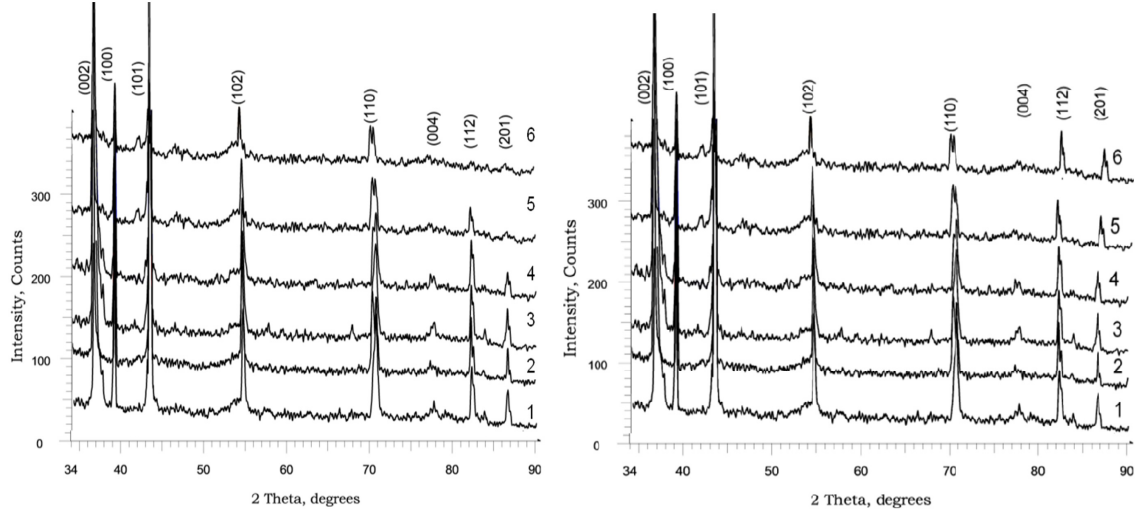

Figure 2. X-ray diffraction patterns of Zn NT samples before and after irradiation with accelerated Xe^{+22} (a) and Kr^{+17} (b) heavy ions: (1) – pristine sample; (2) – 1×10^{9}; (3) – 1×10^{10}; (4) – 1×10^{10}; (5) – 1×10^{11}; (6) – 5×10^{11} m^{-2}.

The summary of XRD data and calculated structural parameters of pristine and irradiated Zn NTs embedded in PET TeMs with different fluencies are presented in Table 1. The average grain sizes L of the pre- and post-irradiated samples were calculated using Scherrer's formula and are compiled in Table 1.

The average crystallite size of the un-irradiated Zn NTs is 16.22 nm, which increases with the increase in xenon and krypton ions irradiation dose and becomes 35.14 and 25.24 nm at the dose of (5×10^{11}) ion/cm^{2}, respectively. The preferred orientation of the crystal lattice planes was found using texture analysis. The preferred orientation of the crystal lattice planes was found using texture analysis. The texture coefficients of preferred orientations were determined by the Harris formula:

$$TC(HKL) = \frac{I(hkl)}{I_0(hkl)} \bigg/ \frac{1}{n} \sum \frac{I(hkl)}{I_0(hkl)}, \tag{1}$$

where $I(hkl)$ is the experimentally obtained relative intensity, $I_0(hkl)$ is the relative intensity corresponding to the given plane according to the JCPDS database, and n is the number of planes. The calculation results are shown in Table 2 and Table 3.

The values of texture coefficient greater than one imply the preferred orientation of nanotube array along the corresponding diffraction planes. Analysis of the texture coefficients showed that the bombardment with studied ions results in slight rearrangement of textural planes, which leads to a decrease in the degree of crystallinity of Zn NTs. The experimental findings revealed that the energy deposited by the ions was not sufficient to cause damage to or decomposition of the grains but was sufficient to induce movement of the granular orientation, as is evident from Tables (2-3). This movement of the planes could be the reason for

the observed changes in the properties of the grain boundaries and the modified structural and electrical properties of the nanotubes.

Table 1.
Structural parameters of pristine and irradiated Zn NTs at different fluences.

Fluence, m^{-2}	Xe^{+22}				Kr^{+17}			
	a,Å	c,Å	c/a	L, nm	a,Å	c,Å	c/a	L, nm
pristine	2.664	4.914	1.843	16.22±1.5	2.664	4.9137	1.843	16.22±1.5
1.0E+09	2.666	4.918	1.845	16.84±1.2	2.665	4.9183	1.846	17.54±1.2
1.0E+10	2.665	4.927	1.848	18.31±0.8	2.664	4.9231	1.848	19.21±0.8
5.0E+10	2.663	4.927	1.849	25.13±1.5	2.663	4.9265	1.850	21.23±1.5
1.0E+11	2.665	4.929	1.850	30.08±0.9	2.665	4.9281	1.850	23.13±0.9
5.0E+11	2.664	4.926	1.851	35.14±1.1	2.664	4.9263	1.849	25.24±1.1

Table 2.
The texture values corresponding to the different planes of Zn NTs exposed with Xe^{+22} ions.

Fluence, m^{-2}	Planes							
	(002)	(100)	(101)	(102)	(110)	(004)	(112)	(201)
pristine	1.46	0.94	1.54	0.93	0.71	0.62	0.85	0.60
1.0E+09	1.34	0.87	1.46	0.88	0.86	0.52	0.89	0.54
1.0E+10	1.23	0.91	1.37	0.76	0.89	0.70	0.41	0.5
5.0E+10	1.13	1.01	1.34	0.82	0.61	0.64	0.31	0.32
1.0E+11	1.00	0.67	1.43	0.76	0.51	-	0.24	-
5.0E+11	1.3	0.55	1.34	0.65	0.50	-	-	-

Table 3.
The texture values corresponding to the different planes of Zn NTs exposed with Kr^{+17} ions.

Fluence, m^{-2}	Planes							
	(002)	(100)	(101)	(102)	(110)	(004)	(112)	(201)
pristine	1.46	0.94	1.54	0.93	0.71	0.62	0.85	0.60
1.0E+09	1.41	0.91	1.52	0.89	0.68	0.58	0.79	0.56
1.0E+10	1.46	0.98	1.51	0.89	0.65	0.55	0.89	0.54
5.0E+10	1.42	0.99	1.53	0.85	0.63	0.53	0.78	0.51
1.0E+11	1.31	0.98	1.58	0.84	0.58	0.51	0.75	0.43
5.0E+11	1.66	0.79	1.61	0.79	0.54	0.48	0.62	0.39

Figure 3 (a-b) shows I-U curves for the Zn NTs before and after irradiation with Xe^{+17} and Kr^{+17} ions. In case of Xe^{+17} ions with the increasing radiation dose, the conductivity decreases and at fluence greater than (5×10^{10}) m^{-2}., polyvacancy complexes and amorphous phase nuclei begin to form. As a result, energy barriers between the disordered regions and the conductive surface emerge in the structure [18]. The magnitude of the barrier depends on the radiation dose and is determined by the size and properties of disordered regions, which impede the movement of electrons. The disordered regions themselves also act as an additional electron scattering factor, resulting in a decrease in conductivity of nanostructures after irradiation with xenon ions.
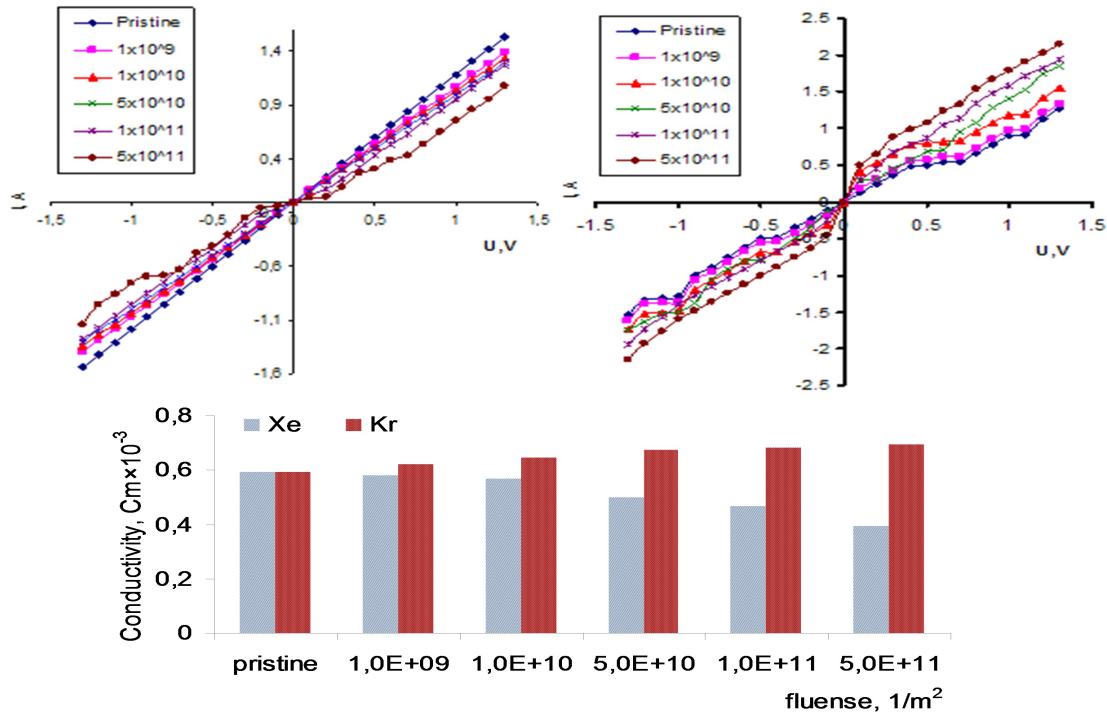
Figure 3. X-ray diffraction patterns of Zn NT samples before and after irradiation with accelerated Xe $^{+22}$ (a) and Kr $^{+17}$ (b) heavy ions: (1) – pristine sample; (2) – 1×10^{9} ; (3) – 1×10^{10} ; (4) – 1×10^{10} ; (5) – 1×10^{11} ; (6) – 5×10^{11} m $^{-2}$.

Heavy ions induced modification of nanostructures can bring significant change in their transport behavior as a result of modification of crystal structure caused by increase of defects concentration as well as texture planes rearrangement.

The most vital parameters of any ion beam process are the energy of the ion governing the range and implantation profile, the ion fluence and the substrate temperature facilitating the rearrangement processes. In general, energetic ions on impinging, pass through the surface of a material and give up their energy by collisions with the atoms ('nuclear stopping') and the electronic system ('electronic stopping'). The first effect gives rise to defects - mainly Frenkel pair point defects - and also the formation of an implantation cascade within very small time scales of femtoseconds. Ion energy, ion mass and target density decides the volume of this collision cascade.

The ion energy introduced in this small volume is partially and ultimately transferred to phonons, resulting in the dissipation of the energy to the surrounding material very quickly. The latter process gives rise to ionization process in the nanostructure thereby increasing the number of free charge carriers, which are then transported under the applied bias. The energy deposited by the implanted ions is not easily dissipated in the confined nanostructures as fast as in bulk or thin film systems. Due to high energy of Kr ion and on its passage through nanowires, it will produce ionization effect thereby increasing the amount of charge carriers. The energy of implanted ion is imparted to the target material after its collision with electrons and nuclei of the target material. Both electronic and nuclear loss contributes in localized heating. If the target atom acquires sufficient energy to leave its position, then various defects like interstitial pairs, va-

cancies, point defects etc may produce in the target [19]. The creation of defects thereby increasing the concentration of charge carriers, consequently enhancing the conductivity of the Zn NTs after irradiation with krypton ions (figure 3b). So, due to the retainment of induced local heating and greater dynamic annealing, implanted Kr-ions may have got slowly diffused into the sample creating more charge carriers and thus, the concentration of intrinsic and thermally generated charge carriers may have risen. This results in the enhancement in conductivity on implantation.

Conclusion

In summary, zinc nanotubes of 380 nm diameter, synthesized by template electrodeposition technique in PET track etched membranes, were irradiated using 1.75 MeV Xe and Kr ions beam at fluencies ranging from (1×10^9) to (5×10^{11}) ions/cm^2. In case of Xe^{+17} ions with the increasing radiation dose, the conductivity decreases and at fluence greater than (5×10^{10}) m^{-2} polyvacancy complexes and amorphous phase nuclei begin to form. As a result, energy barriers between the disordered regions and the conductive surface emerge in the structure. The enhancing the conductivity of the Zn NTs after irradiation with krypton ions was caused by the creation of defects increasing the concentration of charge carriers.

Thus, the SHI irradiations change the conductivity of nanostructures effectively and may be used in heavy ion irradiation environment by exploring the possibilities of different ion energies, fluencies, and incident ions beams.

References

[1] P. Guo et al., Nano Lett. **10** (2010) 2202-2206.
[2] C. Shen et al., Sci. Rep. **3** (2013) 2294.
[3] A. Cultrera et al., J. Phys. D. Appl. Phys. **47** (2014) 015102(1-8).
[4] R. Choudhary et al., J Mater Sci: Mater Electron. **27** (2016) 11674-11681.
[5] D. Shikhaal et al., J Mater Sci: Mater Electron. **28** (2017) 2487-2493.
[6] B. Bushra et al., Curr. Appl. Phys. **15** (2015) 642-647.
[7] A. Kaur et al., Radiat. Eff. Defects Solids. **169** (2014) 513-521.
[8] P. Rana et al., Physica B. **451** (2014) 26-33.
[9] D. Gehlawat et al., Mater. Chem. Phys. **145** (2014) 60-67.
[10] D. Gehlawat et al., Mater. Res. Bull. **49** (2014) 454-461.
[11] P. Rana et al., Nuclear Instruments and Methods in Physics Research B. **349** (2015) 50-55.
[12] R.P. Chauhan et al., Nuclear Instruments and Methods in Physics Research Section B: Beam Interactions with Materials and Atoms. **379** (2016) 78-84.
[13] D.I. Shlimas et al., High Energ. Chem. **51** (2017) 11-16.
[14] U. Ozgur et al., J. Appl. Phys. **98** (2015) 041301.
[15] Z.L Wang et al., Science. **312** (2006) 242-246.
[16] S.K. Chakarvarti et al., Radiat. Meas. **29** (1998) 149-159.
[17] W.J.E. Beek et al., Adv. Mater. **16** (2004) 1009-1013.
[18] K.K. Choudhary et al., J. Phys. Chem. Solids. **73** (2012) 460-463.
[19] S. Panchal et al., Physics Letters A. **32** (2017) 2636-2642.